IEEE Access
Multidisciplinary | Rapid Review | Open Access Journal

Received August 16, 2019, accepted September 9, 2019, date of publication September 17, 2019, date of current version October 1, 2019.

Digital Object Identifier 10.1109/ACCESS.2019.2941968

Multi-Dimensional Space–Time Shift Keying for Wireless Communications

GUANGTAO ZHENG[1,2] AND MING JIANG[1], (Senior Member, IEEE)
[1]School of Electronics and Information Technology, Sun Yat-sen University, Guangzhou 510275, China
[2]Department of Computer Science, University of Virginia, Charlottesville, VA 22903, USA

Corresponding author: Ming Jiang (jiangm7@mail.sysu.edu.cn)

This work was supported in part by the National Key Research and Development Program of China under Grant 2018YFB1802300, in part by the General Project of National Natural Science Foundation of China under Grant 61771499, in part by the Guangdong Provincial Key Research and Development Project under Grant 2018B010114001, and in part by the Key Research and Development Program on Industrial Technologies of Guangzhou City under Grant 201902010053.

ABSTRACT In this paper, we introduce the concept of multi-dimensional (MD) space-time shift keying (STSK) for improving conventional STSK schemes, while still maintaining the general STSK structure for backward compatibility. Firstly, we design two transmission modes for three-dimensional (3-D) STSK schemes, referred to as R2 3-D STSK and R3 3-D STSK, with the incorporation of 3-D constellations. In addition, we devise a joint optimization mechanism utilizing the modified simplified conjugate gradient (SCG) algorithm to enhance the achievable system performance of R3 3-D STSK, through a harmonized design of the constellation and the dispersion matrix set. Furthermore, we derive the optimal combinations of the 3-D constellation coordinates for R2 3-D STSK by maximizing the minimal determinant of the difference matrices. Then, we extend 3-D STSK to the MD STSK family, offering a flexible and efficient performance enhancement mechanism for STSK systems. Extensive simulation results are provided to show the tradeoffs among link performance, diversity order and signal dimensionality of the proposed MD STSK scheme, illustrating a good way to upgrade conventional STSK systems.

INDEX TERMS Coordinate combination, joint optimization, multi-dimensional constellation, multiple-input multiple-output, space-time shift keying.

I. INTRODUCTION

The space-time shift keying (STSK) [1], [2] modulation scheme is a multiple-input multiple-output (MIMO) [3] technique which may meet the rapidly growing demand for high-rate wireless communications over dispersive fading channels. Exploiting the spatial degree of freedom (DOF), STSK provides a flexible system design method that strikes for an efficient tradeoff between multiplexing and diversity. At the receiver, codeword detection based on the low-complexity single-stream maximum likelihood (ML) principle may be possible [4], since there exists no inter-channel interference (ICI), which in contrast is observed in many multi-stream MIMO systems, such as space division multiplexing (SDM), etc. Furthermore, a generalized STSK (G-STSK) scheme was proposed in [5], extending the STSK concept to a wider framework that subsumes diverse MIMO arrangements, such as linear dispersion code (LDC) [6], [7], spatial modulation (SM) [8], Bell Laboratories layered space-time (BLAST) [9] and orthogonal space-time block codes (OSTBCs) [10], thus making the STSK family an attractive candidate technology for advanced MIMO applications.

Generally speaking, the selection of both a constellation and a dispersion matrix set (DMS) affects the overall performance of STSK systems. On the one hand, from the constellation perspective, it is known that under the same normalized average power, a constellation having a larger minimum Euclidean distance (MED) typically offers better link robustness for a system communicating over the additive Gaussian white noise (AWGN) channel [11]. Furthermore, three-dimensional (3-D) constellations are capable of providing improved MED and hence better performance when compared with their conventional two-dimensional (2-D) counterparts. The 3-D constellations have been used in optical communications [12] and were introduced in orthogonal frequency division multiplexing (OFDM) based wireless communications [13]. Since then, various 3-D constellations were proposed for advanced wireless applications [13]–[17].

The associate editor coordinating the review of this manuscript and approving it for publication was Wasiu Oyewole Popoola.

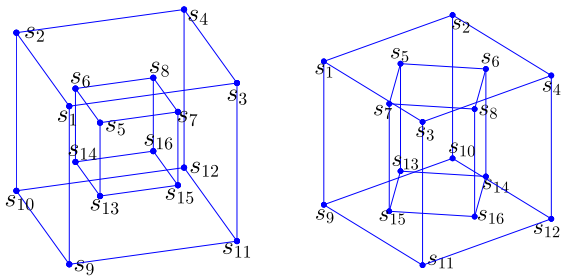

(a)16CIC (b)16RCIC

FIGURE 1. Examples of 16-ary 3-D constellations: 16CIC [14] and 16RCIC [15].

Fig. 1a and Fig. 1b show two examples of 16-ary 3-D constellations, namely the cube-in-cube (CIC) [14] and rotated CIC (RCIC) [15] arrangements, where s_l ($l = 1, \cdots, L$; $L = 16$) denotes a constellation signal point. The construction of high-order 3-D constellations was also proposed [18], while symbol error probabilities of various constellations were analyzed [18], [19]. Furthermore, inspired by 3-D constellations, N-D constellations were developed for further increasing the reliability of link transmissions [11], [20].

On the other hand, several methods have been proposed for optimizing the DMS [4]. However, optimizing the DMS alone may not be the ultimate solution, since the achievable performance of STSK systems also depends on a few other aspects, for example the signal constellation used. This inspired a proposal of joint optimization on both the signal constellation and the DMS [21], which exploits additional DOF attainable by harmonized designs of the constellation and the DMS, and thus provides an enhanced performance.

Recently, under the concept of multi-functional MIMO [22], various schemes, for example the multi-set STSK [23], hierarchical multi-functional layered SM [24], multi-dimensional index modulation [25], etc., tend to explore multiple dimensions to achieve a tradeoff among throughput, error performance and diversity. However, these schemes typically require nontrivial architectural changes and/or the employment of new devices such as the fast antenna switching units, thus raising cost and backward compatibility issues.

Based on this background, in this paper, both multi-dimensional (MD) constellations and the joint optimization mechanism are exploited to form the new MD STSK scheme. The proposed MD STSK approach improves the achievable performance of conventional STSK systems without changing their general structure, thus ensures maximum backward compatibility with existing applications. Specifically, our main contributions include:

1) Given an STSK system, our approach uses reduced-sized DMSs and 3-D constellation symbols with a time division multiplexing (TDD) approach to trade for a better symbol error rate (SER). Specifically, two implementation options, namely the Rate-3 (R3) and Rate-2 (R2) schemes, are suggested for achieving different design tradeoffs among various parameters of 3-D STSK systems.
2) Based on the maximal discrete-input continuous-output memoryless channel (DCMC) capacity criterion, we modify the existing simplified conjugate gradient (SCG) aided joint optimization method, such that it becomes applicable to the proposed R3 3-D STSK systems. Through the resultant new 3-D joint optimization (3DJO) algorithm, the signal constellation and the DMS used in 3-D STSK systems can be jointly optimized, yielding an improved system performance compared with that of the systems dispensing with 3DJO.
3) To our best knowledge, the optimization for STSK systems is conventionally conducted from the DMS or symbol aspect. However, we prove that optimization from the coordinate perspective is also possible and helpful by developing a new algorithm referred to as the optimal coordinate combination search (OCCS). The new OCCS technique optimizes the 3-D coordinates' combinations through maximizing the minimal determinant of the so-called difference matrices for R2 3-D STSK systems.
4) Furthermore, we extend the 3-D STSK framework to the N-dimensional (N-D) case, where we have $N > 3$. This results in the generalized N-D STSK framework, where the aforementioned 3DJO algorithm is also extended to its N-D version. We show that when set up with the same size of STSK codeword or equivalently the same STSK structure, higher-dimensional STSK schemes outperform their lower-dimensional counterparts in terms of error rates, favorably under the same STSK structure and spectral efficiency (SE).
5) Last but not least, assuming the same SE and STSK structure, we provide extensive simulation results which help to offer many insights into the new schemes and to reveal their benefits as well as design tradeoffs, through comparisons among diverse configurations and/or with conventional STSK systems.

The rest of the paper is organized as follows. The 3-D STSK concept is presented in Section II, where two transmission modes, R2 and R3, are first introduced in Section II-A. Then the 3-D STSK framework is proposed in Section II-B, followed by our analysis on the error rate and the DCMC capacity of 3-D STSK in Section II-C and Section II-D, respectively. In Section III, the two optimization algorithms, namely 3DJO and OCCS, are detailed. Next, we extend the 3-D framework to the MD scenario in Section IV, resulting in the generalized MD STSK systems and the MD joint optimization (MDJO) technique. Further, a complexity analysis is given in Section IV-C, while extensive simulation results are provided in Section V to demonstrate the benefits and design tradeoffs of the proposed MD STSK systems. Finally, we conclude our work in Section VI.

For readers' convenience, we summarize the main notations used in this paper as follows. Bold upper (lower) variables denote matrices (vectors); $\otimes$ represents Kronecker

product; tr[·] stands for the trace operation; $(\cdot)^T$ and $(\cdot)^H$ refer to the transpose and Hermitian transpose operations, respectively; $(\cdot)_{:,v}$ (or $(\cdot)_{v,:}$) indicates the selection of the v^{th} column (or row) of a given matrix; $\|\cdot\|$ denotes the Frobenius norm; $\mathbb{E}[\cdot]$ is the expectation operation; $\Re\{\cdot\}$ is defined as getting the real part of a complex number; $\lceil\cdot\rceil$ represents the operation of rounding a float number to the larger and nearest integer.

II. 3-D STSK: CONCEPT AND PRINCIPLES

In this section, we first introduce two 3-D signal transmission modes, and then discuss the proposed 3-D STSK framework corresponding to its two transmission modes.

A. 3-D SIGNAL TRANSMISSION MODES

We define two 3-D signal transmission modes as the *R3 mode* and the *R2 mode* [26], respectively. In the R3 mode, a 3-D symbol duration T_s^{R3} is divided into three equal-sized time slots, each having a duration of $T_s^{\mathrm{R3}}/3$. One time slot accommodates one real-valued coordinate, denoted by x_l, y_l or z_l, of a 3-D symbol selected from a size-L 3-D constellation. The discrete vectorized transmitted symbol therefore becomes

$$\mathbf{s}_l = [k_x x_l, k_y y_l, k_z z_l], \quad l \in \{1, \cdots, L\}, \tag{1}$$

where k_x, k_y and k_z are normalization factors having the value of unity.

In contrast, in the R2 mode, the 3-D symbol duration T_s^{R2} is divided into two equal-sized time slots, each having a duration of $T_s^{\mathrm{R2}}/2$. In the first time slot, two out of the three real-valued coordinates of a 3-D constellation symbol are combined to form a 2-D complex symbol for quadrature transmissions, while the remaining coordinate is transmitted in the next consecutive time slot as a real symbol. This results in the so-called *transformed* 3-D constellation symbol

$$\acute{\mathbf{s}}_l = [k_x x_l + j k_y y_l, k_z z_l], \tag{2}$$

where we set $k_x = k_y = \sqrt{3/4}$ and $k_z = \sqrt{3/2}$ to even the average transmitted symbol power in each of the two time slots. This is beneficial for power amplifier (PA) implementation. Obviously, there exist a total of 6 transformed 3-D constellations that correspond to the 6 coordinate combinations, respectively. In Section III-B, we will demonstrate how to optimize the design, from the coordinate perspective, of enhanced 3-D STSK schemes.

Note that assuming the same time slot duration of $T_s = T_s^{\mathrm{R2}}/2 = T_s^{\mathrm{R3}}/3$ or equivalently the same system bandwidth, the R3 and R2 modes require three-fold and two-fold transmission time in comparison to the conventional 2-D signal transmission mode, respectively. The increased transmission time per 3-D symbol results in a smaller dispersion matrix (DM) size based on the same STSK structure. We will show in Section V that the above designs together help to significantly improve the achievable link performances against the 2-D counterpart, when the joint optimization approach is employed.

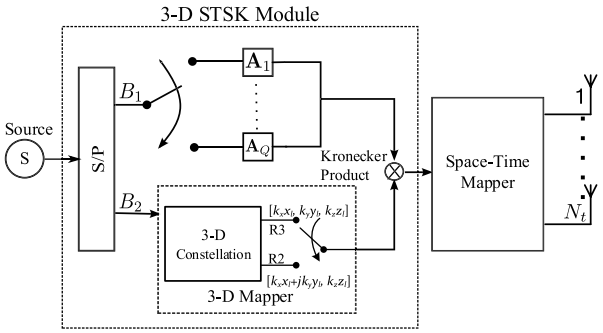

FIGURE 2. The illustration of the proposed 3-D STSK module.

B. 3-D STSK FRAMEWORK

The proposed 3-D STSK module is illustrated in Fig. 2. The input information bit sequence of size $B_I = B_1 + B_2$ is divided into two portions. The first B_1 bits are used to select one DM out of the predefined DMS denoted by $\{\mathbf{A}_q | q = 1, \cdots, Q\}$, where $Q = 2^{B_1}$ denotes the cardinality of the DMS. Different from the conventional STSK design [1], the remaining B_2 bits are mapped to one of $L = 2^{B_2}$ constellation symbols $\mathbf{s}_l$ ($l = 1, \cdots, L$) by a 3-D mapper. The selected constellation symbol is then dispersed through space and time by the selected DM $\mathbf{A}_q$ through Kronecker product, resulting in a 3-D STSK codeword $\mathbf{S}_{q,l}$. Each row and each column of $\mathbf{S}_{q,l}$ correspond to a transmit antenna and a time slot of duration T_s, respectively. In fact, the 3-D STSK module shown in Fig. 2 can be implemented by a look-up table (LUT), where the STSK codewords are indexed by the B_I input bits. Thus, the proposed 3-D STSK process can be seamlessly integrated with the general STSK transmitter.

For convenience, we denote the configuration of a proposed 3-D STSK system as (N_t, N_r, T_B, Q, R), where N_t is the number of transmit antennas, N_r is the number of receive antennas, T_B is the number of columns in a DM satisfying $T = T_B R$, where T is an integer denoting the time duration of a STSK codeword normalized to T_s, and $R = \{2, 3\}$ denotes the 3-D STSK transmission mode. Fig. 3 shows an example of the R3 3-D STSK transmitter with configuration (3, 2, 2, 16, 3), employing the 3-D 16CIC mapper of [14]. This configuration shares the same structure as the conventional STSK of (3, 2, 6, 16, 1), where the last parameter $R = 1$ refers to the 2-D case. Note that all DMs are dimensioned 3-by-2, and the resultant STSK codeword is a 3-by-6 matrix.

As seen in Fig. 3, the i^{th} STSK codeword can be generated by the dispersion operation

$$\mathbf{S}(i) = \mathbf{S}_{q,l}^{(i)} = \mathbf{A}_q^{(i)} \otimes \mathbf{s}_l^{(i)}, \tag{3}$$

where we have $\mathbf{A}_q^{(i)} \in \mathcal{C}^{N_t \times T_B}$, $\mathbf{s}_l^{(i)} \in \Omega$, and Ω is a 3-D constellation symbol set. Note that each of the Q predefined DMs, $\mathbf{A}_q^{(i)}$ ($q = 1, \cdots, Q$), should satisfy the power constraint of $\mathrm{tr}[\mathbf{A}_q^{(i)} \cdot (\mathbf{A}_q^{(i)})^H] = T_B$ [1]. Note that the columns of a STSK codeword are transmitted from the first to the last, for example from 1 to 6 in the specific 3-D STSK configuration example of Fig. 3. However, in order to facilitate our

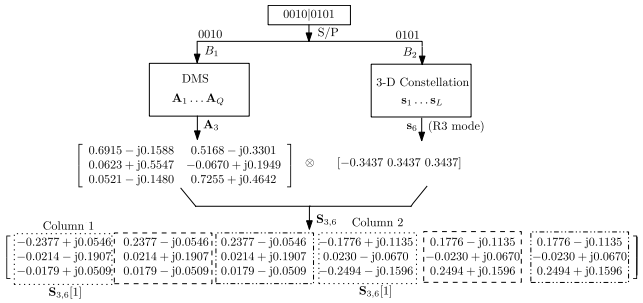

FIGURE 3. Exemplification of the 16CIC-aided 3-D STSK(3,2,2,16,3) scheme, where a pair of two columns (accommodated by boxes of the same line style) in the big codeword matrix $\mathbf{S}_{3,6}$ belongs to $\mathbf{S}(i)[v]$, $v \in \{1, \dots, R\}$, as formulated in (4).

analysis next, we reform (3) as

$$\mathbf{S}(i)[v] = \mathbf{s}_l^{(i)}[v]\mathbf{A}_q^{(i)}, \quad v = 1, \dots, R, \tag{4}$$

where $\mathbf{s}_l^{(i)}[v]$ is the v^{th} element of a R2 or R3 3-D symbol. Then, the received signal can be represented by

$$\mathbf{Y}(i)[v] = \mathbf{H}(i)[v]\mathbf{S}(i)[v] + \mathbf{Z}(i)[v], \quad v = 1, \dots, R, \tag{5}$$

where $\mathbf{H}(i)[v] \in \mathcal{C}^{N_r \times N_t}$ is the channel matrix with each element having a zero mean and unit variance of independent and identically distributed (i.i.d.) complex Gaussian distribution $\mathcal{CN}(0, 1)$. We assume that the channel is frequency-flat Rayleigh fading and that $\mathbf{H}(i)[v] = \mathbf{H}(i)$ $(v = 1, \dots, R)$ remains unchanged during one codeword duration. The variable $\mathbf{Z}(i)[v] \in \mathcal{C}^{N_r \times T_B}$ in (5) denotes the AWGN matrix with each element following the distribution $\mathcal{CN}(0, N_0)$, where N_0 is the complex noise variance for each time slot T_s. By applying the vec$(\cdot)$ operation [1] to (5), we have

$$\overline{\mathbf{Y}}(i)[v] = \overline{\mathbf{H}}(i)\chi(\mathbf{K}(i))_{:,v} + \overline{\mathbf{Z}}(i)[v], \quad v = 1, \dots, R, \tag{6}$$

where

$$\overline{\mathbf{Y}}(i)[v] = \text{vec}(\mathbf{Y}(i)[v]) \in \mathcal{C}^{N_r T_B \times 1}, \tag{7}$$
$$\overline{\mathbf{H}}(i) = \mathbf{I} \otimes \mathbf{H}(i) \in \mathcal{C}^{N_r T_B \times N_t T_B}, \tag{8}$$
$$\overline{\mathbf{Z}}(i)[v] = \text{vec}(\mathbf{Z}(i)[v]) \in \mathcal{C}^{N_r T_B \times 1}, \tag{9}$$
$$\chi = [\text{vec}(\mathbf{A}_1), \cdots, \text{vec}(\mathbf{A}_Q)] \in \mathcal{C}^{N_t T_B \times Q}, \tag{10}$$

and $\mathbf{I}$ is the $(T_B \times T_B)$-dimensional identity matrix. Furthermore, $\mathbf{K}(i) = \mathbf{K}_{q,l}^{(i)} \in \mathcal{C}^{Q \times R}$ in (6) is the equivalent transmit signal matrix defined by

$$\mathbf{K}(i) = \underbrace{\begin{bmatrix} 0 \cdots 0 & x_l^{(i)} & 0 \cdots 0 \\ 0 \cdots 0 & y_l^{(i)} & 0 \cdots 0 \\ 0 \cdots 0 & z_l^{(i)} & 0 \cdots 0 \end{bmatrix}^T}_{q-1 \qquad\qquad Q-q}, \tag{11}$$

for R3 3-D STSK, and

$$\mathbf{K}(i) = \underbrace{\begin{bmatrix} 0 \cdots 0 \\ 0 \cdots 0 \end{bmatrix}}_{q-1} \underbrace{\begin{matrix} \sqrt{3/4}(x_l^{(i)} + j y_l^{(i)}) \\ \sqrt{3/2}\, z_l^{(i)} \end{matrix}}_{} \underbrace{\begin{bmatrix} 0 \cdots 0 \\ 0 \cdots 0 \end{bmatrix}^T}_{Q-q}, \tag{12}$$

for R2 3-D STSK, respectively, where $[x_l^{(i)}, y_l^{(i)}, z_l^{(i)}]$ refer to the coordinates of the l^{th} 3-D symbol. Note that for each 3-D symbol duration, there exist a total number of $Q \cdot L$ legitimate transmit signal matrices $\mathbf{K}_{q,l}^{(i)}$ $(q = 1, \cdots, Q;\ l = 1, \cdots, L)$.

On the receiver side of the proposed 3-D STSK system, the optimal maximum likelihood (ML) detector is employed. Assuming perfect channel state information (CSI), the transmitted 3-D symbol and the selected DM can be jointly estimated by

$$\begin{aligned}(\hat{q}, \hat{l}) &= \arg \min_{q,l} \sum_{v=1}^{R} \| \overline{\mathbf{Y}}(i)[v] - \overline{\mathbf{H}}(i)\chi(\mathbf{K}(i))_{:,v} \|^2 \\ &= \arg \min_{q,l} \sum_{v=1}^{R} \| \overline{\mathbf{Y}}(i)[v] - \mathbf{s}_l^{(i)}[v] \left(\overline{\mathbf{H}}(i)\chi\right)_{:,q} \|^2. \end{aligned} \tag{13}$$

C. PAIRWISE ERROR PROBABILITY

In this section, the upper bound of the pairwise error probability (PEP) of the 3-D STSK system is analyzed. We define

$$D = \prod_{n=1}^{r} \lambda_n, \tag{14}$$

as the difference matrix distance (DMD), where λ_n $(n = 1, \cdots, r)$ and r are the nonzero eigenvalues and the rank of matrix $\mathbf{A} = \Delta\Delta^H$, respectively. The difference matrix Δ is defined by

$$\Delta = \mathbf{S}_{q,l} - \mathbf{S}_{q',l'} = \mathbf{A}_q \otimes \mathbf{s}_l - \mathbf{A}_{q'} \otimes \mathbf{s}_{l'}, \tag{15}$$

where $q, q' \in \{1, \cdots, Q\}$ and $l, l' \in \{1, \cdots, L\}$. For notation brevity, we have ignored the 3-D STSK codeword index i in (15). Moreover, depending on the relations between l, l', q and q', there can be three categories of symbol errors in 3-D STSK systems, namely E_1, E_2 and E_3, defined by

$$\begin{aligned} E_1 &= \{l \neq l',\ q = q'\}, \\ E_2 &= \{l = l',\ q \neq q'\}, \\ E_3 &= \{l \neq l',\ q \neq q'\}. \end{aligned} \tag{16}$$

Inspired by [27], the upper bound of PEP of a 3-D STSK codeword $\mathbf{S}_{q,l}$ at a high signal-to-noise ratio (SNR) may be derived as

$$P(\mathbf{S}_{q,l} \to \mathbf{S}_{q',l'}) \leq \left(\frac{1}{4N_0}\right)^{-rN_r} \cdot D^{-N_r}. \tag{17}$$

Note from (17) that given a fixed N_r, the PEP's upper bound depends on r and D. Based on the rank-and-determinant design criterion [28], in most cases the $N_t \times N_t$ matrix $\mathbf{A}$ is full rank, thus we have $r = N_t$. This implies that the achievable symbol error performance of the 3-D STSK system is dominated by the value of DMD.

Furthermore, given that $\mathbf{A}$ is full rank, D can be equivalently written as (18), as shown at the top of the next page according to [29] and with the aid of (16). Therefore, the parameters employed by (18), namely both the MED and the constellation symbol's power ρ_l defined by

$$\rho_l = \mathbf{s}_l \mathbf{s}_l^H = \|\mathbf{s}_l\|^2, \quad l = 1, \cdots, L, \tag{19}$$

$$D = \begin{cases} [(\mathbf{s}_l - \mathbf{s}_{l'})(\mathbf{s}_l - \mathbf{s}_{l'})^H]^{N_t} \det(\mathbf{A}_q \mathbf{A}_q^H), & \text{for } E_1 \\ (\mathbf{s}_l \mathbf{s}_l^H)^{N_t} \det[(\mathbf{A}_q - \mathbf{A}_{q'})(\mathbf{A}_q - \mathbf{A}_{q'})^H], & \text{for } E_2 \\ \det[(\mathbf{A}_q \otimes \mathbf{s}_l - \mathbf{A}_{q'} \otimes \mathbf{s}_{l'})(\mathbf{A}_q \otimes \mathbf{s}_l - \mathbf{A}_{q'} \otimes \mathbf{s}_{l'})^H], & \text{for } E_3 \end{cases} \tag{18}$$

can be used as two key performance indicators for the proposed STSK system, as to be revealed in Section V.

D. DCMC CAPACITY

The DCMC capacity is restricted to a given type of constellations, and it is different from Shannon capacity which is based on continuous-input continuous-output memoryless (CCMC) channels. The DCMC capacity defined for MIMO channels in conjunction with MD constellations can be found in [30]. Moreover, the DCMC capacity of a conventional STSK scheme is developed in [2] as

$$\begin{aligned} C_{\text{DCMC}} &= \frac{1}{T_B} \max_{p(\mathbf{K}_{1,1}),\cdots,p(\mathbf{K}_{Q,L})} \sum_{q,l} \int_{-\infty}^{\infty} \cdots \int_{-\infty}^{\infty} p(\overline{\mathbf{Y}}|\mathbf{K}_{q,l}) \\ &\quad \cdot p(\mathbf{K}_{q,l}) \log_2 \left[\frac{p(\overline{\mathbf{Y}}|\mathbf{K}_{q,l})}{\sum_{q',l'} p(\overline{\mathbf{Y}}|\mathbf{K}_{q',l'}) p(\mathbf{K}_{q',l'})} \right] d\overline{\mathbf{Y}} \text{ (bit/symbol)}, \end{aligned} \tag{20}$$

where the conditional probability for 2-D constellations is formulated by

$$p(\overline{\mathbf{Y}}|\mathbf{K}_{q,l}) = \frac{1}{(\pi N_0)^{N_r T_B}} \exp\left(- \frac{\left\| \overline{\mathbf{Y}} - \overline{\mathbf{H}} \chi \mathbf{K}_{q,l} \right\|^2}{N_0} \right). \tag{21}$$

Assume that all legitimate symbols for transmissions are equiprobable, then we have $p(\mathbf{K}_{q,l}) = \frac{1}{Q \cdot L}$ ($q = 1, \cdots, Q$; $l = 1, \cdots, L$). Next, through replacing the integration in (20) by expectation, we can obtain

$$\begin{aligned} C_{\text{DCMC}} = \frac{1}{T_B} \Bigg[\log_2 (Q \cdot L) - \frac{1}{Q \cdot L} \\ \cdot \sum_{q,l} E \left[\log_2 \left\{ \sum_{q',l'} \exp\left(\Psi_{q,l}^{q',l'} \right) | K_{q',l'} \right\} \right] \Bigg]. \end{aligned} \tag{22}$$

Thanks to a compatible signal structure, the DCMC capacity of the proposed 3-D STSK system can be computed by using its 2-D version given in (22), with the variable $\Psi_{q,l}^{q',l'}$ modified as (23), as shown at the top of the next page. Depending on the value of R, the signal matrix $\mathbf{K}_{q,l}$ in (23) associated with the 3-D STSK mode should follow the definition in (11) or (12). Note that the derived DCMC capacity will be exploited for the optimization process in Section III.

III. 3-D STSK OPTIMIZATION

Based on the new 3-D STSK framework introduced in Section II, we now propose two optimization algorithms for improving the achievable performances of 3-D STSK systems.

A. 3-D JOINT OPTIMIZATION

Recall from (18) that both the signal constellation and the DMS affect the DMD, and thus have an impact on the system's performance. Joint optimization on both domains helps to exploit maximal DOF from these aspects for potential performance enhancements. The joint optimization algorithm for 2-D STSK in terms of maximizing the DCMC capacity based on the SCG principle [21] can achieve a good tradeoff between convergence speed and computational complexity [31]. Inspired by the approach targeting 2-D constellations [21], in the sequel we extend it to 3-D STSK systems as the new 3-D joint optimization (3DJO) algorithm.

More specifically, we first randomly generate N_{RD} constellations and the corresponding DMSs, and then compute the DCMC capacity for each DMS-constellation pair (DCP). Naturally, the DCP yielding the maximal capacity will be identified, which includes the initial candidate DMS $\chi(1)$ defined in (10) and the initial candidate constellation $\Omega(1)$. Next, we calculate the gradients $\mathbf{F}(1,1) = \nabla_\chi C_{\text{DCMC}}(\chi(1), \Omega(1)) \in \mathcal{C}^{N_t T_B \times Q}$ and $\mathbf{J}(1,1) = \nabla_\Omega C_{\text{DCMC}}(\chi(1), \Omega(1)) \in \mathcal{C}^{3 \times L}$, where the numbers in the round brackets of $\mathbf{F}(1,1)$ and $\mathbf{J}(1,1)$ denote the DMS index and the constellation index, respectively. Moreover, we define the gradient operators $\nabla_\chi = \left[\frac{\partial}{\partial[(\chi)_{:,1}]} \cdots \frac{\partial}{\partial[(\chi)_{:,Q}]} \right]$ and $\nabla_\Omega = \left[\frac{\partial}{\partial[(\Omega)_{:,1}]} \cdots \frac{\partial}{\partial[(\Omega)_{:,L}]} \right]$.

Then, we set the initial search directions, namely $\mathbf{D}(1) = \mathbf{F}(1,1)$ from the DMS aspect, and $\mathbf{G}(1) = \mathbf{J}(1,1)$ from the constellation aspect. During the iterative processing procedure, based on a finite positive step μ, new constellations and DMSs are simultaneously generated towards the iteratively updated search directions and then normalized. An averaging window of size L_c, where L_c is a positive integer, is used for facilitating the termination of the iterative search. After the algorithm terminates, the DMS and the constellation generated in the final iteration are considered as the final joint solution. The 3DJO algorithm is outlined in Algorithm 1.

If we define $\nabla_{\chi[m]} = \frac{\partial}{\partial[(\chi)_{:,m}]}$ and $\nabla_{\Omega[k]} = \frac{\partial}{\partial[(\Omega)_{:,k}]}$, then according to [21], the theoretical value of $\nabla_{\chi[m]} C_{\text{DCMC}}$ is

$$\begin{aligned} &\nabla_{\chi[m]} C_{\text{DCMC}} \\ &= -\frac{1}{T_B Q L} \mathbb{E}\left[\sum_{q=1}^{Q} \sum_{l=1}^{L} \frac{\sum_{q'=1}^{Q} \sum_{l'=1}^{L} \exp(\Psi_{q,l}^{q',l'}) \nabla_{\chi[m]} \Psi_{q,l}^{q',l'}}{\ln 2 \cdot \sum_{q'=1}^{Q} \sum_{l'=1}^{L} \exp(\Psi_{q,l}^{q',l'})} \right]. \end{aligned} \tag{24}$$

$$\Psi_{q,l}^{q',l'} = \frac{1}{N_0}\sum_{v=1}^{R}\left\{ -\left\|\overline{\mathbf{H}}\chi\left[(\mathbf{K}_{q,l})_{:,v} - (\mathbf{K}_{q',l'})_{:,v}\right] + \overline{\mathbf{Z}}[v]\right\|^2 + \left\|\overline{\mathbf{Z}}[v]\right\|^2\right\}$$
$$= \frac{1}{N_0}\sum_{i=1}^{N_r}\sum_{v=1}^{R}\left\{ -\left\|(\overline{\mathbf{H}}\chi)_{i,:}\left[(\mathbf{K}_{q,l})_{:,v} - (\mathbf{K}_{q',l'})_{:,v}\right] + (\overline{\mathbf{Z}}[v])_{i,:}\right\|^2 + \left\|(\overline{\mathbf{Z}}[v])_{i,:}\right\|^2\right\} \quad (23)$$

Algorithm 1 3-D Joint Optimization (3DJO) Algorithm

1: **Input:** $\chi(1)$, $\Omega(1)$, $\mathbf{D}(1)$, $\mathbf{G}(1)$, $\mu > 0$, $\varepsilon > 0$, $L_c \in \mathbb{Z}^+$, $\beta(1) = \|\mathbf{F}(1,1)\| + \|\mathbf{J}(1,1)\|$, $i = 1$
2: **repeat**
3: $\chi(i+1) = \chi(i) + \mu\mathbf{D}(i)$
4: $[\chi(i+1)]_{:,q} = \sqrt{T_B}\frac{[\chi(i+1)]_{:,q}}{\|[\chi(i+1)]_{:,q}\|}(q = 1, \cdots, Q)$
5: $\Omega(i+1) = \Omega(i) + \mu\Re\mathfrak{e}\{\mathbf{G}(i)\}$
6: $\Omega(i+1) = \sqrt{L}\frac{\Omega(i+1)}{\|\Omega(i+1)\|}$
7: $\phi_i = \frac{\|\mathbf{F}(i+1,i+1)\|^2}{\|\mathbf{F}(i,i+1)\|^2}$
8: $\mathbf{D}(i+1) = \phi_i\mathbf{D}(i) + \mathbf{F}(i+1,i+1)$
9: $\psi_i = \frac{\|\mathbf{J}(i+1,i+1)\|^2}{\|\mathbf{J}(i,i+1)\|^2}$
10: $\mathbf{G}(i+1) = \psi_i\mathbf{G}(i) + \mathbf{J}(i+1,i+1)$
11: $\beta(i+1) = \|\mathbf{F}(i+1,i+1)\| + \|\mathbf{J}(i+1,i+1)\|$
12: $i = i+1$
13: **if** $i < 2L_c$ **then**
14: **goto** 3
15: **end if**
16: **until** $\varepsilon > \frac{1}{L_c}\left|\sum_{k=i-L_c+1}^{i}\beta(k) - \sum_{k=i-2L_c+1}^{i-L_c}\beta(k)\right|$
17: **Output:** Joint solution $\{\chi(i), \Omega(i)\}$

In (24), note that the theoretical gradients $\nabla_{\chi[m]}\Psi_{q,l}^{q',l'}$ $(m = 1, \cdots, Q)$ for 3-D STSK, where $\Psi_{q,l}^{q',l'}$ is defined in (23) with $R = 3$, need to be computed first by

$$\nabla_{\chi[m]}\Psi_{q,l}^{q',l'}$$
$$= -\frac{1}{N_0}\sum_{v=1}^{3}\nabla_{\chi[m]}\left\{\overline{\mathbf{H}}\chi\left[(\mathbf{K}_{q,l})_{:,v} - (\mathbf{K}_{q',l'})_{:,v}\right] + \overline{\mathbf{Z}}[v]\right\}^H$$
$$\times\left\{\overline{\mathbf{H}}\chi\left[(\mathbf{K}_{q,l})_{:,v} - (\mathbf{K}_{q',l'})_{:,v}\right] + \overline{\mathbf{Z}}[v]\right\}$$
$$= -\frac{2}{N_0}\sum_{v=1}^{3}\left[(\mathbf{K}_{q,l})_{:,v}^H - (\mathbf{K}_{q',l'})_{:,v}^H\right]_{:,m}\overline{\mathbf{H}}^H$$
$$\times\left\{\overline{\mathbf{H}}\chi\left[(\mathbf{K}_{q,l})_{:,v} - (\mathbf{K}_{q',l'})_{:,v}\right] + \overline{\mathbf{Z}}[v]\right\}. \quad (25)$$

Through a similar way as (24), the value of $\nabla_{\Omega[k]}C_{\mathrm{DCMC}}$ can be derived, where $\nabla_{\Omega[k]}\Psi_{q,l}^{q',l'}$ $(k = 1, \cdots, L)$ is given by

$$\nabla_{\Omega[k]}\Psi_{q,l}^{q',l'} = -\frac{2}{N_0}\left\{\delta_{k,l}(\overline{\mathbf{H}}\chi)_{:,q} - \delta_{k,l'}(\overline{\mathbf{H}}\chi)_{:,q'}\right\}^H$$
$$\times\left\{\overline{\mathbf{H}}\chi(\mathbf{K}_{q,l} - \mathbf{K}_{q',l'}) + \overline{\mathbf{Z}}\right\}, \quad (26)$$

and $\delta_{k,l}$ is defined as

$$\delta_{k,l} = \begin{cases} 1, & k = l \\ 0, & k \neq l. \end{cases} \quad (27)$$

As seen in Line 16 of Algorithm 1, a small positive parameter ε is exploited in the termination criterion of 3DJO. In order to track the convergence of 3DJO, a sliding window of size $2L_c$ is invoked, where the block of the latest L_c values of β, and the preceding block of the same size, are respectively averaged and the difference between them is calculated. If the difference is smaller than ε, convergence is detected and the 3DJO algorithm terminates. The computational complexity of Algorithm 1 measured in terms of the number of real multiplications, is on the order of $\mathcal{O}(N_r T_B R Q^3 L^2 (L + Q + N_t T_B) N_{mc} N_{th})$, where N_{mc} is the number of Monte Carlo samples used to approximate the expectation in (24), and N_{th} is the maximum number of iterations.

Furthermore, it is worth mentioning that Algorithm 1 is only applicable to R3 3-D STSK for the following reasons. The search direction $\mathbf{G}(i)$ associated with the constellation aspect is generally complex-valued, while the constellation $\Omega(i)$ to be optimized is either real (R3 mode) or partly real (R2 mode). Thus, gradient projection is naturally needed in order to match the data types of $\mathbf{G}(i)$ and $\Omega(i)$ in Algorithm 1. For R3 3-D STSK systems, the constellation $\Omega(i)$ contains real symbols only, hence the $\Re\mathfrak{e}\{\cdot\}$ operation seen in Line 5 of Algorithm 1 is invoked to force $\mathbf{G}(i)$ to be real. This operation may be considered as projecting the search direction $\mathbf{G}(i)$ onto a lower-dimensional space without diverging from the original direction.

However, in R2 3-D STSK systems where transformed constellations exemplified in (2) are used, the first and second rows of $\Omega(i)$ are complex and real, respectively. If the gradient projection operation only forces the second row of $\mathbf{G}(i)$ to be real while keeping the first row of complex data unchanged, the overall search direction may become somewhat rotated, which might result in some divergence of the optimization process. Hence, the 3DJO algorithm may not be directly applicable to R2 3-D STSK as to R3 3-D STSK.

Nonetheless, in fact the jointly optimized DCP generated by 3DJO for R3 3-D STSK, can also be employed in R2 3-D STSK for performance enhancements, as evidenced in Section V. Having said that, we further introduce the so-called OCCS algorithm designed particularly for R2 3-D STSK, as detailed next.

B. OPTIMAL COORDINATE COMBINATION SEARCH

Recall that in R2 3-D STSK, the transformed constellation symbols are created by combining the coordinates of 3-D symbols in a given 3-D constellation, as indicated by (2). More explicitly, for any given 3-D constellation to be used in

Algorithm 2 Optimal Coordinate Combination Search (OCCS) Algorithm

1: **Input:** $\mathbb{C}$, $N_{\mathbb{C}}$ and $i = 1$
2: **repeat**
3: Select $\mathbb{C}(i)$, and for all legitimate values of l, l', q and q', compute all possible sets: $\Theta = \{ D \mid E_1 \text{ or } E_2 \text{ or } E_3 \}$, where E_j ($j = 1, 2, 3$) are defined in (16) and D is computed using (14)
4: $D_{\min}(i) = \min(\Theta)$
5: $i = i + 1$
6: **until** $i > N_{\mathbb{C}}$
7: $m_{D_{\min}} = \arg\{\max_i [D_{\min}(i)]\}$
8: **Output:** Optimal coordinate combination $\mathbb{C}(m_{D_{\min}})$

TABLE 1. The minimal DMD values $D_{\min}$ computed for coordinate combinations upon all values of q and l, using 3-D constellations 16CIC [14] and 16RCIC [15] in R2 3-D STSK.

Coordinate Combinations	$D_{\min}$	
	16CIC	16RCIC
$(z + jy, x)$	0.0277	0.0368
$(z + jx, y)$	0.0277	0.0368
$(y + jz, x)$	0.0277	0.0368
$(y + jx, z)$	0.0277	0.0399
$(x + jy, z)$	0.0277	0.0399
$(x + jz, y)$	0.0277	0.0368

R2 3-D STSK, the values of ρ_l defined in (19) and the MED may vary subjected to the specific transformed constellation employed, or equivalently to the arbitrary legitimate coordinate combinations representing the transformed symbols. Hence, we opt to minimize the PEP upper bound of (17), which is affected by the DMD, as discussed in Section II-C. This clue therefore inspires us to maximize the minimal DMD through appropriate selection of coordination combinations for R2 3-D STSK, yielding the proposed OCCS algorithm described by Algorithm 2, where $D_{\min}$ is the minimal DMD, $\mathbb{C}$ is the set of all coordinate combinations suggesting how the coordinates are combined with each other, and $N_{\mathbb{C}}$ is the cardinality of $\mathbb{C}$. The computational complexity of Algorithm 2 is on the order of $\mathcal{O}(Q^2L^2T_BRN_t^4N!)$, where $N = 3$ is the constellation dimensionality.

As an example, in Table 1 we summarize the results computed for a R2 3-D STSK system employing the 16CIC [14] and 16RCIC [15] constellations of Fig. 1. Note that in the coordinate combinations seen in Table 1, the power normalization factors $\{k_x, k_y, k_z\}$ mentioned in Section II-A are not shown for notation simplicity.

From Table 1, we can see that for 16CIC, the values of $D_{\min}$ are the same for all coordinate combinations. This is expected, since the structure of this specific 3-D constellation is symmetric from the perspectives of coordinate axes $\overrightarrow{x}$, $\overrightarrow{y}$ and $\overrightarrow{z}$, as seen in Fig. 1. In contrast, note that for the 16RCIC-aided R2 3-D STSK, the minimal DMD values associated with combinations $(x + jy, z)$ and $(y + jx, z)$ are larger than those associated with other combinations. This fact indicates that these two specific combinations are the best in terms of the DMD criterion under the given R2 3-D STSK configuration. It also implies that the proposed OCCS algorithm is beneficial for 3-D constellations having irregular or asymmetric structures. Numerical results validating our arguments based on Table 1 are provided in Section V. Note however that OCCS does not apply to R3 3-D STSK systems, where no transformed constellation can be applied.

IV. EXTENSION TO MD STSK

In this section, the proposed 3-D STSK framework, the 3DJO as well as the OCCS techniques are extended and generalized to MD STSK systems, followed by the complexity analysis.

A. MD STSK FRAMEWORK

MD STSK employs an N-D constellation. We reuse the notation of (N_t, N_r, T_B, Q, R) to represent MD STSK configurations. Similar to 3-D STSK which supports two transmission modes of R2 and R3, in MD STSK we have two transmission modes of RN and R$\lceil \frac{N}{2} \rceil$. More explicitly, the R$N$ scheme divides the N-D symbol duration T_s^{RN} into N equal-sized time slots, each accommodating one coordinate of a specific N-D symbol. In contrast, the R$\lceil \frac{N}{2} \rceil$ scheme combines two coordinates of the N-D symbol into a transformed complex constellation symbol. If N is odd, then the last time slot will be allocated the only remaining coordinate as a real symbol, otherwise each time slot will be allocated a complex symbol formed by a coordinate pair. Each time slot has the same duration T_s, thus an N-D symbol will require N-fold and approximately $\frac{N}{2}$-fold of transmission time for RN and R$\lceil \frac{N}{2} \rceil$ modes, respectively, as compared to a 2-D symbol. Here we omit the mathematical model of N-D STSK, since it can be readily extended from 3-D STSK.

Furthermore, the formulas for computing the DCMC capacity of MD STSK are consistent with (22) and (23). More specifically, in (23), we may set $R = N$ and $R = \lceil \frac{N}{2} \rceil$ for computing the DCMC capacity of RN and R$\lceil \frac{N}{2} \rceil$ N-D STSK systems, respectively.

B. OPTIMIZED MD STSK

Thanks to the similar signal structure, the OCCS algorithm developed for R2 3-D STSK in Section III-B can be directly applied to R$\lceil \frac{N}{2} \rceil$ N-D STSK with appropriately selected coordinate combinations.

On the other hand, the 3DJO algorithm of Section III-A can be extended to the so-called MD joint optimization (MDJO) algorithm without significant changes. To elaborate further, Algorithm 1 can be readily reused in RN N-D STSK and in R$\lceil \frac{N}{2} \rceil$ N-D STSK with N being even, where in the latter case, $\Omega(i)$ seen in Algorithm 1 becomes a pure complex matrix and thus Line 5 of Algorithm 1 should be changed to

$$\Omega(i + 1) = \Omega(i) + \mu \mathbf{G}(i). \tag{28}$$

When N is odd in R$\lceil \frac{N}{2} \rceil$ N-D STSK, for similar reasons as the R2 3-D STSK case, MDJO is not directly applicable.

However, the N-D constellations optimized by MDJO targeting the RN mode can also be used for improving the performance of R$\lceil \frac{N}{2} \rceil$ mode, where OCCS can always be enabled for achieving additional gains.

Concerning the proposed MDJO algorithm for RN ($N = 4, 5, 6, \cdots$) and R$\lceil \frac{N}{2} \rceil$ ($N = 4, 6, 8, \cdots$) systems, where we have $R = N$ and $R = \frac{N}{2}$ respectively, $\nabla_m \Psi_{q,l}^{q',l'}$ of (25) should be generalized to

$$\nabla_{\chi[m]} \Psi_{q,l}^{q',l'} = -\frac{2}{N_0} \sum_{v=1}^{R} \left[(\mathbf{K}_{q,l})_{:,v}^H - (\mathbf{K}_{q',l'})_{:,v}^H \right]_{:,m} \overline{\mathbf{H}}^H \times \left[\overline{\mathbf{H}} \chi [(\mathbf{K}_{q,l})_{:,v} - (\mathbf{K}_{q',l'})_{:,v}] + \overline{\mathbf{Z}}[v] \right]. \quad (29)$$

C. COMPLEXITY ANALYSIS

Assuming that the ML detection is invoked at the receiver, the computational complexity per bit measured by the number of real multiplications in conventional 2-D STSK can be derived by [1]

$$\mathfrak{C}_{2D} = \frac{N_r T_B Q (4 N_t T_B + 6L)}{\log_2(QL)}, \quad (30)$$

where $4N_t T_B N_r T_B Q$ real multiplications are needed for computing $\overline{\mathbf{H}}(i)\chi$, $4N_r T_B QL$ real multiplications are needed for computing $\mathbf{s}_l^{(i)}[v] \left(\overline{\mathbf{H}}(i)\chi \right)$, and $2N_r T_B QL$ real multiplications are needed for computing the vector norm in (13) with $R = 1$ for the 2-D case.

Note that we have assumed that one complex multiplication and one computation of the absolute value of a complex number are equivalent to four and two real multiplications, respectively. Thus, given a 2-D constellation, the term $\mathbf{s}_l^{(i)}[v]\chi$ can be computed offline, since it is invariant to CSI. This computation takes $4N_t T_B QL$ real multiplications once for all, since we can store the offline results in an LUT for later use. Additionally, another $4N_t T_B N_r T_B Q$ and $2N_r T_B QL$ real multiplications are needed for computing $\mathbf{s}_l^{(i)}[v] \left(\overline{\mathbf{H}}(i)\chi \right)$ and the vector norm, respectively.

For the N-D case, the computational complexity for the repeated process is the same as that in the 2-D case, given that the STSK codewords have the same period. To build the LUT, $2N_t \overline{T}_B QLN = 2N_t T_B QL$ real multiplications are needed for RN MD STSK, where $\overline{T}_B = T_B/N$ is the number of columns in a DM for RN. For the R$\lceil \frac{N}{2} \rceil$ case, with the time slot $\widetilde{T}_B$ satisfying $\lceil \frac{N}{2} \rceil \widetilde{T}_B = T_B$, we have the following two cases:

1) if N is odd, then a number of $4N_t \widetilde{T}_B \lfloor N/2 \rfloor QL + 2N_t \widetilde{T}_B QL = 4N_t T_B QL - 2N_t \widetilde{T}_B QL$ real multiplications are needed.
2) if N is even, the required number of real multiplications is $4N_t T_B QL$.

In the MD STSK family, the computational complexity varies, though the RN-based schemes have lower complexities than the R$\lceil \frac{N}{2} \rceil$-based counterparts. In any case, the proposed MD STSK scheme operates as an enhancement to conventional 2-D STSK systems, imposing little additional computational complexity for signal detection.

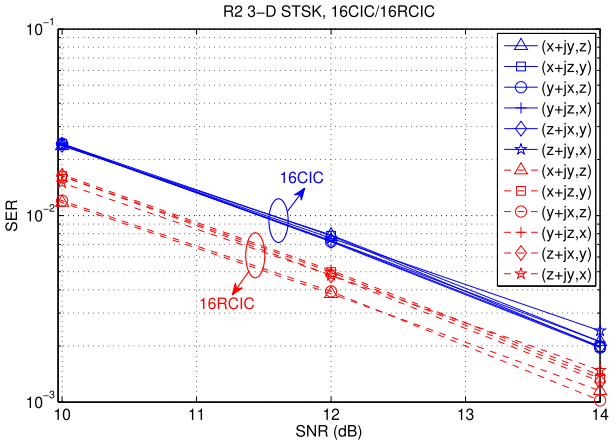

FIGURE 4. SER performance comparison of various coordinate combinations for R2 3-D STSK system employing 16CIC or 16RCIC.

V. PERFORMANCE RESULTS

In this section, link-level performance results of 3-D/N-D STSK systems with various configurations are provided and compared with their conventional 2-D counterparts. The design tradeoff between time diversity, link performance and constellation dimensionality is also discussed. Since many of the parameters employed by the STSK systems are mutually dependent, some of them, such as the constellation size, the numbers of transmit and receive antennas, and the cardinality of DMS are fixed for all schemes investigated, in order to facilitate fair comparisons between various schemes and/or configurations. Furthermore, the ML detector and i.i.d. frequency-flat Rayleigh fading channels with perfect CSI are assumed.

As our first investigation, Fig. 4 shows the impact from the OCCS algorithm in an example 3-D STSK(3,2,2,16,2) system, where the 3-D constellation 16CIC or 16RCIC given in Fig. 1 is employed. As expected, it is observed from Fig. 4 that all coordinate combinations for 16CIC provide a similar performance because of the symmetric structure of the specific constellation. In contrast, it reveals that the coordinate combinations $(x+jy, z)$ and $(y+jx, z)$ produce the best SER performance for 16RCIC, which complies with our theoretical analysis in Section III-B. Such results prove that the additional new DOF extracted from the coordinate aspect indeed helps to further improve the achievable performance of 3-D STSK systems for selected 3-D constellations. In the remaining part of this section, we will use the coordinate combination of $(x + jy, z)$ to generate the results for the R2 3-D STSK system employing 16CIC or 16RCIC.

Next, in Fig. 5 we compare the SER performances of 3-D STSK and conventional 2-D STSK systems using 16-ary constellations, namely the popular 2-D 16-ary quadrature amplitude modulation (16QAM) and 3-D 16CIC/16RCIC. The configurations for all schemes yielding the same SE of 4/3 bps/Hz are detailed in Table 2. The DMS for each scheme was obtained by random search according to the rank-and-determinant criterion [28]. Fig. 5 shows that given

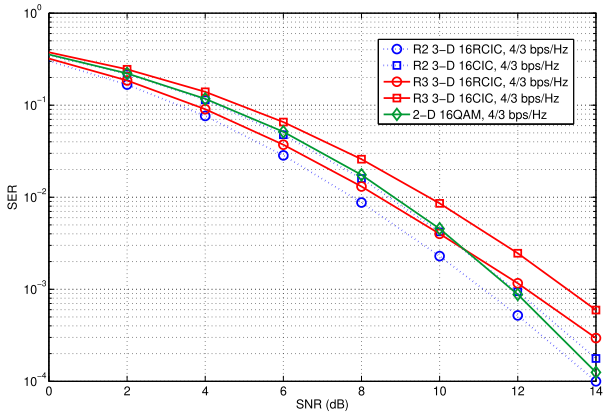

FIGURE 5. Performance comparison of 2-D STSK and 3-D STSK systems in terms of SER.

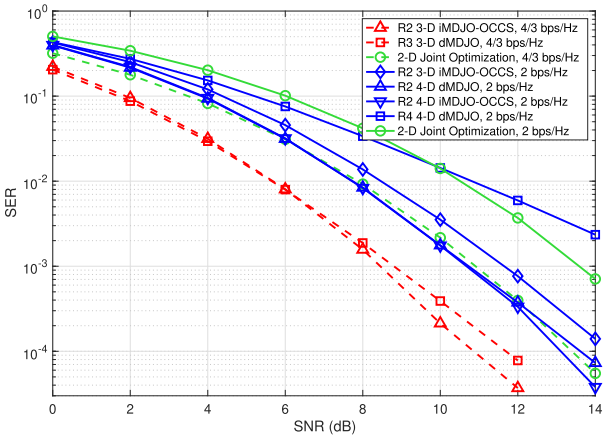

FIGURE 6. Performance comparison of 3-D STSK and 4-D STSK systems in terms of SER.

TABLE 2. Configurations for 2-D/3-D STSK without joint optimization.

Configuration	Constellation
3-D STSK(3,2,2,16,3)	16RCIC
3-D STSK(3,2,2,16,3)	16CIC
3-D STSK(3,2,3,16,2)	16RCIC
3-D STSK(3,2,3,16,2)	16CIC
2-D STSK(3,2,6,16,1)	16QAM

the same constellation, the R2-aided scheme outperforms the R3 arrangement. Furthermore, at the same SE of 4/3 bps/Hz, employing the 3-D 16RCIC constellation helps to improve the system's link robustness in comparison to the conventional 2-D scheme under low-to-medium SNRs below 10 dB. However, note that all the 3-D schemes in Fig. 5 do not employ the 3DJO algorithm in Section III-A. This in fact limits their achievable system performances, especially for R3 16CIC 3-D STSK, which performs even worse than the 2-D scheme.

Hence, in a further study, we evaluate the performances of the STSK systems supporting the proposed 3DJO, MDJO and/or OCCS algorithms. As an example, we set $N = \{3, 4\}$ in the N-D STSK schemes and fix the size of constellations to 16, while assuming an SE of 4/3 bps/Hz or 2 bps/Hz. Detailed configurations are given in Table 3, where the conventional joint optimization approach [21] is applied to the 2-D STSK benchmark.

Recall from Section IV-B that MDJO is only applicable to RN, or to R$\lceil \frac{N}{2} \rceil$ with N being even. In both cases, MDJO is referred to as direct-MDJO (dMDJO), which is applicable to all N-D STSK schemes in Table 3, except the R2 3-D STSK scheme which is unable to exploit MDJO due to its specific asymmetric structure, as pointed out in Section IV-B. Nonetheless, we apply the 3-D DCP optimized through MDJO and invoke OCCS in R2 3-D STSK, where such a combination is referred to as indirect MDJO with OCCS (iMDJO-OCCS). More specifically, in the MDJO algorithm we set $N_{\mathrm{RD}} = 100, \mu = 5, L_c = 15$ and $\varepsilon = 0.001$. In order to avoid local convergence, ϕ_i and ψ_i were set to 0 after every 10 iterations, such that only the current gradients are used for updating the constellation and DMS. Through preliminary tests, interestingly, we found that the performances of various MD DCPs generated by MDJO are not very sensitive to a wide range of SNR values. Hence, in full simulations we opted for optimizing the MD DCPs with a fixed SNR value of 0 dB for all STSK configurations invoking MDJO.

Based on Table 3, we plot the SER performances of various STSK schemes in Fig. 6. We can see that for the same targeted SE of 4/3 or 2 bps/Hz, the optimized MD STSK significantly outperforms the optimized 2-D STSK. These results imply that given the same STSK codeword duration,

TABLE 3. Configurations for 2-D/3-D/4-D STSK with joint optimization.

bps/Hz	Configuration	Algorithm	DCP source
4/3	3-D STSK(3,2,3,16,2)	iMDJO-OCCS	3-D STSK(3,2,3,16,3)
	3-D STSK(3,2,2,16,3)	dMDJO	Direct optimization
	2-D STSK(3,2,6,16,1)	2DJO	Direct optimization
2	3-D STSK(3,2,2,16,2)	iMDJO-OCCS	3-D STSK(3,2,2,16,3)
	4-D STSK(3,2,2,16,2)	dMDJO	Direct optimization
	4-D STSK(3,2,2,16,2)	iMDJO-OCCS	4-D STSK(3,2,2,16,4)
	4-D STSK(3,2,1,16,4)	dMDJO	Direct optimization
	2-D STSK(3,2,4,16,1)	2DJO	Direct optimization

TABLE 4. Comparison of MED and $\rho_{\min}$ values of various 3-D constellations assuming the SE of 4/3 bps/Hz.

Constellation	16CIC		16RCIC		Optimized	
Algorithm	OCCS	-	OCCS	-	iMDJO-OCCS	dMDJO
Mode	R2	R3	R2	R3	R2	R3
MED	0.486	0.687	0.522	0.738	0.727	0.836
$\rho_{\min}$	0.354	0.191	0.681	0.545	0.756	0.992

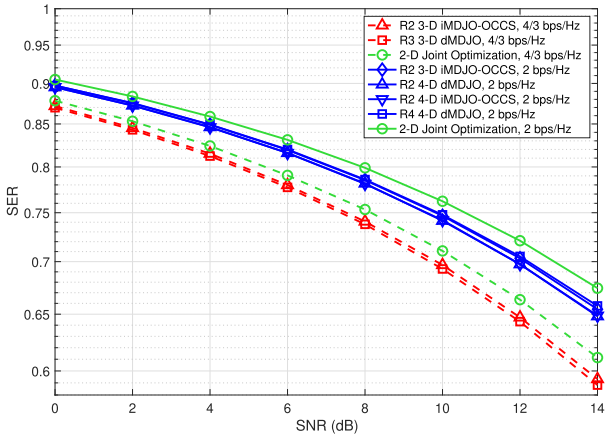

FIGURE 7. Performance comparison of 3-D STSK and 4-D STSK systems in terms of SER over a 28GHz mmW channel.

trading the time diversity for signal dimensionality can help to achieve a better link performance for STSK. For example, in both 3-D STSK(3,2,2,16,3) and 2-D STSK(3,2,6,16,1), the STSK codeword matrices have the same dimension of 3×6, yielding the same STSK codeword duration. However, a 3-D STSK(3,2,2,16,3) codeword is produced by a 3-D symbol and a 3×2 DM, while a 2-D STSK(3,2,6,16,1) codeword is generated by a 2-D complex symbol and a larger 3×6 DM. As a result, 3-D STSK(3,2,2,16,3) outperforms 2-D STSK(3,2,6,16,1), as evidenced in Fig. 6.

On the other hand, performance improvements may be achieved, when we trade for higher time diversity by combining the coordinates of signal points in high dimensional constellations through the proposed OCCS technique. As evidenced from Fig. 6, 3-D STSK(3,2,3,16,2) outperforms 3-D STSK(3,2,2,16,3), and 4-D STSK(3,2,2,16,2) outperforms 4-D STSK(3,2,1,16,4), respectively. Note that as mentioned in Section IV-B, dMDJO cannot be directly applied to R2 3-D schemes. However, with OCCS, we can not only achieve such performance gains dispensing with dMDJO, but also save the offline efforts for DCP optimization. From Fig. 6, it is shown that performances of R2 4-D dMDJO and R2 4-D iMDJO-OCCS are very similar. This implies that with the aid of OCCS, we may directly apply the coordinate-combined version of the specific DCP which is optimized for R4 4-D, to the R2 4-D scheme without resorting to dMDJO.

Moreover, Fig. 6 shows that under a similar STSK configuration, increasing the constellation's dimension from 3-D to 4-D yields a better performance. More explicitly, when MDJO is invoked, R2 4-D STSK outperforms R2 3-D STSK. However, note that R4 4-D STSK performs worse than its 2-D counterpart when SNR exceeds 10 dB. This phenomenon suggests that there exists some optimal tradeoff between time diversity and signal dimensionality in MD STSK systems, which requires further studies.

Recall from the end of Section II-C that both the MED and the minimum 3-D symbol power, which we define here as $\rho_{\min} = \min_l(\rho_l)$ with ρ_l $(l = 1, \cdots, L)$ given by (19), affect the overall performance of STSK systems. As an example, we summarize both metrics for the 3-D 16CIC/16RCIC and 3-D dMDJO/iMDJO-OCCS R2 constellations in Table 4, where all schemes have the same SE of 4/3 bps/Hz. From the table, we observe that under the same transmission mode R, the new constellations generated by the proposed optimization algorithms typically have larger MED and $\rho_{\min}$ values than the conventional 16CIC/16RCIC constellations. This in turn brings the performance benefits of our proposed schemes, as exhibited by the simulation results. Therefore, we may conclude that given a fixed STSK codeword duration, the proposed MD STSK schemes offer a beneficial way to strike for an effective tradeoff among various design parameters, such as the signal dimensionality, the targeted link performance as well as time diversity.

In addition, in Fig. V we plot the SER performance over the more realistic millimeter wave (mmW) channel model offered by the NYUSIM simulator [32], where uniform linear arrays with 3 transmit antennas and 2 receive antennas are used. We assume a carrier frequency of 28GHz under the non-line-of-sight (NLOS) environment with the distance between the transmitter and the receiver ranging from 10m to 200m. Other parameters remain to be their default values set by the channel model. It is observed from Fig. V that although our proposed scheme is not specifically optimized for operations in such an environment, it still performs better than the reference arrangements. Further designs of new schemes optimized for mmW channels with the aid of wideband technologies, such as OFDM, will be part of our future endeavors.

VI. CONCLUSION

In this paper, a MD constellation aided STSK framework exploiting different transmission modes was proposed. Furthermore, two optimization algorithms, namely MDJO and OCCS, were designed to improve the attainable performances of MD STSK. Both theoretical analyses and simulation results were provided. It was shown that the proposed scheme outperformed conventional 2-D STSK systems and could strike for a beneficial tradeoff among various design parameters, such as the signal dimensionality, the targeted link performance as well as time diversity, thanks to its

optimized DCP. Our future work will consider an adaptive mechanism switching between different STSK configurations, in an attempt to approach the optimal tradeoff with respect to the various aspects.

REFERENCES

[1] S. Sugiura, S. Chen, and L. Hanzo, "Coherent and differential space-time shift keying: A dispersion matrix approach," *IEEE Trans. Commun.*, vol. 58, no. 11, pp. 3219–3230, Nov. 2010.

[2] S. Sugiura, S. Chen, and L. Hanzo, "A universal space-time architecture for multiple-antenna aided systems," *IEEE Commun. Surveys Tuts.*, vol. 14, no. 2, pp. 401–420, 2nd Quart., 2012.

[3] M. Jiang and L. Hanzo, "Multiuser MIMO-OFDM for next-generation wireless systems," *Proc. IEEE*, vol. 95, no. 7, pp. 1430–1469, Jul. 2007.

[4] S. Sugiura, "Dispersion matrix optimization for space-time shift keying," *IEEE Commun. Lett.*, vol. 15, no. 11, pp. 1152–1155, Nov. 2011.

[5] S. Sugiura, S. Chen, and L. Hanzo, "Generalized space-time shift keying designed for flexible diversity-, multiplexing- and complexity-tradeoffs," *IEEE Trans. Wireless Commun.*, vol. 10, no. 4, pp. 1144–1153, Apr. 2011.

[6] B. Hassibi and B. M. Hochwald, "High-rate codes that are linear in space and time," *IEEE Trans. Inf. Theory*, vol. 48, no. 7, pp. 1804–1824, Jul. 2002.

[7] M. Jiang and L. Hanzo, "Unitary linear dispersion code design and optimization for MIMO communication systems," *IEEE Signal Process. Lett.*, vol. 17, no. 5, pp. 497–500, May 2010.

[8] R. Mesleh, H. Haas, C. W. Ahn, and S. Yun, "Spatial modulation —A new low complexity spectral efficiency enhancing technique," in *Proc. Int. Conf. Commun. Netw. China (ChinaCom)*, Oct. 2006, pp. 1–5.

[9] G. J. Foschini, "Layered space-time architecture for wireless communication in a fading environment when using multi-element antennas," *Bell Labs Tech. J.*, vol. 1, no. 2, pp. 41–59, Feb. 1996.

[10] V. Tarokh, N. Seshadri, and A. R. Calderbank, "Space-time codes for high data rate wireless communication: Performance criterion and code construction," *IEEE Trans. Inf. Theory*, vol. 44, no. 2, pp. 744–765, Mar. 1998.

[11] B. Sklar, *Digital Communications: Fundamentals and Applications*, 2nd ed. Upper Saddle River, NJ, USA: Prentice-Hall, 2001.

[12] S. Benedetto and P. Poggiolini, "Theory of polarization shift keying modulation," *IEEE Trans. Commun.*, vol. 40, no. 4, pp. 708–721, Apr. 1992.

[13] S. G. Kang, "An OFDM with 3-D signal mapper and 2-D IDFT modulator," *IEEE Commun. Lett.*, vol. 12, no. 12, pp. 871–873, Dec. 2008.

[14] Z. Chen, J. S. Bae, S.-K. Chung, J.-W. Koh, and S. G. Kang, "Multi-envelope 3-dimensional constellations for polarization shift keying modulation," in *Proc. IEEE Int. Conf. Inform. Commun. Technol. Converg. (ICTC)*, Nov. 2010, pp. 173–174.

[15] S. Cho and S. K. Park, "Improved 16-ary constellation mapping for three-dimensional OFDM systems," *Electron. Lett.*, vol. 48, no. 9, pp. 530–532, Apr. 2012.

[16] H. G. Batshon, I. B. Djordjevic, L. L. Minkov, L. Xu, T. Wang, and M. Cvijetic, "Proposal to achieve 1 Tb/s per wavelength transmission using three-dimensional LDPC-coded modulation," *IEEE Photon. Technol. Lett.*, vol. 20, no. 9, pp. 721–723, May 1, 2008.

[17] B. Chen and M. Jiang, "Design of three-dimensional constellations for wireless communication systems," in *Proc. IEEE Int. Conf. Commun. (ICC)*, Jun. 2015, pp. 2876–2881.

[18] S. G. Kang, Z. Chen, J. Y. Kim, J. S. Bae, and J.-S. Lim, "Construction of higher-level 3-D signal constellations and their accurate symbol error probabilities in AWGN," *IEEE Trans. Signal Process.*, vol. 59, no. 12, pp. 6267–6272, Dec. 2011.

[19] Z. Chen and S. G. Kang, "Probability of symbol error of OFDM system with 3-Dimensional signal constellations," in *Proc. IEEE Int. Symp. Consum. Electron. (ISCE)*, May 2009, pp. 442–446.

[20] J.-E. Porath and T. Aulin, "Design of multidimensional signal constellations," *IEEE Proc.- Commun.*, vol. 150, no. 5, pp. 317–323, Oct. 2003.

[21] S. Sugiura and L. Hanzo, "On the joint optimization of dispersion matrices and constellations for near-capacity irregular precoded space-time shift keying," *IEEE Trans. Wireless Commun.*, vol. 12, no. 1, pp. 380–387, Jan. 2013.

[22] M. El-Hajjar and L. Hanzo, "Multifunctional MIMO systems: A combined diversity and multiplexing design perspective," *IEEE Wireless Commun.*, vol. 17, no. 2, pp. 73–79, Apr. 2010.

[23] I. A. Hemadeh, M. El-Hajjar, S. Won, and L. Hanzo, "Multi-set space-time shift-keying with reduced detection complexity," *IEEE Access*, vol. 4, pp. 4234–4246, 2016.

[24] I. A. Hemadeh, M. El-Hajjar, and L. Hanzo, "Hierarchical multi-functional layered spatial modulation," *IEEE Access*, vol. 6, pp. 9492–9533, 2018.

[25] S. Lu, I. A. Hemadeh, M. El-Hajjar, and L. Hanzo, "Compressed sensing-aided multi-dimensional index modulation," *IEEE Trans. Commun.*, vol. 67, no. 6, pp. 4074–4087, Jun. 2019.

[26] G. Zheng and M. Jiang, "Three-dimensional space-time shift keying with coordinate combination and joint optimisation," in *Proc. IEEE Int. Conf. Commun. China (ICCC)*, Nov. 2015, pp. 1–5.

[27] H. Jafarkhani, *Space-Time Coding: Theory and Practice*. Cambridge, U.K.: Cambridge Univ. Press, 2005.

[28] B. Vucetic and J. Yuan, *Space-Time Coding*. Hoboken, NJ, USA: Wiley, 2003.

[29] K. B. Petersen and M. S. Pedersen. (Nov. 2012). *The Matrix Cookbook*. [Online]. Available: http://www2.imm.dtu.dk/pubdb/p.php?3274

[30] S. X. Ng and L. Hanzo, "On the MIMO channel capacity of multidimensional signal sets," *IEEE Trans. Veh. Technol.*, vol. 55, no. 2, pp. 528–536, Mar. 2006.

[31] S. Chen, A. K. Samingan, B. Mulgrew, and L. Hanzo, "Adaptive minimum-BER linear multiuser detection for DS-CDMA signals in multipath channels," *IEEE Trans. Signal Process.*, vol. 49, no. 6, pp. 1240–1247, Jun. 2001.

[32] S. Sun, G. R. MacCartney, and T. S. Rappaport, "A novel millimeter-wave channel simulator and applications for 5G wireless communications," in *Proc. IEEE Int. Conf. Commun. (ICC)*, May 2017, pp. 1–7.

GUANGTAO ZHENG received the B.Sc. degree in electronic information science and technology from Sun Yat-sen University, Guangzhou, China, in 2015, and the M.Eng. degree in electronics and communication engineering from the University of Science and Technology of China, Hefei, China, in 2018. He is currently pursuing the Ph.D. degree in computer science with the University of Virginia, Charlottesville, VA, USA. His research interests include wireless communications, signal processing in large networks, and machine learning.

MING JIANG (M'07–SM'13) received the B.Eng. and M.Eng. degrees from the South China University of Technology (SCUT), China, and the Ph.D. degree from the University of Southampton, U.K., all in electronic engineering. He has substantial international and industrial experience with Fortune 500 telecom companies. From 2006 to 2013, he had held key research and development and/or management positions at the Samsung Electronics Research Institute (SERI), U.K., Nortel Networks' Research and Development Centre, China, and telecom equipment maker New Postcom, China, where he actively participated in numerous collaborative projects, including European FP6 WINNER-II, European FP7 DAVINCI, Mobile WiMAX (IEEE802.16m), and 3GPP LTE/LTE-A standardization across the EU, North America, and Asia, on researching and designing novel algorithms, telecommunication standards, and radio access and core network products. Since June 2013, he has been a Full Professor and a Ph.D. Supervisor with Sun Yat-sen University, China, where he focuses on both scientific research and technology transfer with industrial partners. He has coauthored or contributed to five Wiley books, more than 50 articles in prestigious international journals and conferences, more than 60 patents, and more than 400 3GPP/IEEE standardization contributions. His research interest includes a wide range of areas in next-generation wireless mobile communications. He was a recipient of several Chinese Council Awards, in 2011, including Innovative Leading Talents, Outstanding Experts, and Top Overseas Scholars.